

## Charge structure of multiparticle final states in $pp$ collisions at 102 and 400 GeV/c\*

C. Bromberg, D. Chaney, T. Ferbel, T. Jensen, R. Schindler,<sup>†</sup> P. Slattery, and D. Weingarten  
*University of Rochester, Rochester, New York 14627*

A. A. Seidl and J. C. VanderVelde  
*University of Michigan, Ann Arbor, Michigan 48104*  
 (Received 18 February 1975)

We investigate the distribution of charge in events produced by  $pp$  collisions at 102 and 400 GeV/c. The data are from exposures of the Fermi National Accelerator Laboratory 30-in. bubble chamber. A comparison of the energy dependence of the data with Monte Carlo simulations of random charge distributions provides support for the hypothesis of local compensation of charge. Results on charge transfer are in qualitative agreement with predictions of an independent neutral-cluster emission model.

### I. INTRODUCTION

A detailed investigation of the charge structure of many-particle events has been proposed as a source of useful information concerning the underlying mechanism of particle production.<sup>1-6</sup> Thus, for example, the behavior of the charge transfer  $u$  (defined for  $pp$  collisions as half the difference between the charges in the forward and backward hemispheres of the center-of-mass system) has been examined to test fragmentation models<sup>1</sup> and multiperipheral models<sup>2,3</sup> of particle production. In the first part of the present investigation we will analyze our data in terms of a generalization of the  $u$  variable as suggested by Krzywicki and Weingarten, to obtain evidence concerning the hypothesis of "local compensation of charge" (LCC).<sup>4-7</sup> Then we will compare the inclusive and semi-inclusive behaviors of  $u$  itself with the predictions of a particular model which fulfills the LCC hypothesis, namely the neutral-cluster emission model of Quigg and Thomas.<sup>2</sup>

The generalization of  $u$  used in Refs. 4-6 is a function of rapidity  $Z(y)$ , called a zone graph. For an event with  $N$  charged particles  $Z(y)$  is given by

$$Z(y) = \sum_{i=1}^N q_i \theta(y - y_i) - q_{\text{beam}} \theta(y - y_{\text{beam}}) - q_{\text{target}} \theta(y - y_{\text{target}}), \quad (1)$$

where  $q_i$  is the charge of the particle  $i$  and  $\theta(y - y_i)$  is the usual step function given by 0 for negative arguments and 1 elsewhere. Thus  $-Z(y)$  is the charge transfer across the rapidity value  $y$ . (Zone graphs are illustrated in Fig. 1.) Regions of  $y$  over which  $Z(y)$  remains positive (negative) are called zones of positive (negative) polarity; gaps of no charge transfer ( $Z=0$ ) separate each successive pair of zones. A distinction will be made between "end" zones containing

either beam or target particles ("compensating" charges) and "central" zones containing only final-state particles.

The LCC hypothesis, in one formulation, requires that for sufficiently large values of the energy in the center-of-mass system ( $\sqrt{s}$ ) (1) the internal structure of zones, partially specified for example by the mean zone length  $\langle \lambda_z \rangle$  and the mean number of charges per zone  $\langle n_z \rangle$ , becomes independent of  $s$ , (2) correlations between pairs of zones decrease quickly with increasing separation in rapidity space, and (3) the mean number of zones,  $\langle N_z \rangle$ , grows with energy as  $\ln s$ .<sup>4</sup> Although these conditions are similar to the short-range-order (SRO) hypothesis, they are not identical: A collection of events including diffractive production channels would not fulfill SRO but might, nonetheless, exhibit local compensation of charge.

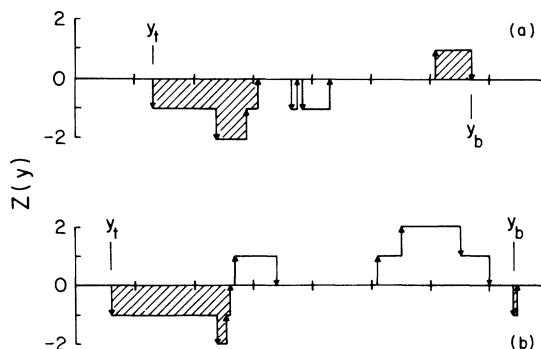


FIG. 1. Zone graphs for two typical events: (a) an 8-prong at 102 GeV/c, (b) a 10-prong at 400 GeV/c. The graph is drawn with positive charges as upward-pointing arrows and negative charges as downward-pointing arrows. The end zones, which contain the beam ( $y_b$ ) and target ( $y_t$ ) rapidities entering as negative charges, are shaded.

In Sec. II, we will test the LCC hypothesis by comparing the charge structure of measured events with the charge structure of a set of fictitious events obtained by randomly reassigning charges to the observed particle tracks. The characteristics of this "randomized charge model" (RCM), which conserves total charge but randomizes the charge distribution of the experimental data, will be used whenever simple theoretical expressions for random behavior are unavailable.

The data to be presented are from approximately 3000 measurements of inelastic  $p\bar{p}$  collisions at 102 GeV/c and from 2200 measurements of collisions at 400 GeV/c. The events were observed in exposures of the Fermilab 30-inch bubble chamber to extracted proton beams of machine energy. The experimental procedures at 102 GeV/c are described in previously published work.<sup>8</sup> Similar analysis procedures were employed for the data at 400 GeV/c. The major source of systematic error is the lack of particle-identification information for particles having laboratory momenta in excess of 1.2 GeV/c. (This region of uncertainty corresponds to  $x = p_{\parallel}^*/p_{\text{max}}^* \gtrsim -0.5$  for protons, where  $p_{\parallel}^*$  and  $p_{\text{max}}^*$  are the center-of-mass values for the longitudinal momentum of the final-state particle and the incident momentum, respectively.) For a given measured momentum, the value of a particle's rapidity is affected by the choice of mass hypothesis; in particular, a pion mass assignment for high-momentum protons causes, typically, an upward shift of  $\sim 0.7$  in rapidity. The cross section for pion production at large  $|x_{\pi}|$  is small compared to that for proton production, and this fact permits us to assign, with great assurance, the proton mass to all positively charged tracks which yield reconstructed values of  $x_{\pi}$  greater than 0.6. This procedure diminishes somewhat the uncertainty in  $y$  due to proton/pion mass ambiguity for  $y \gtrsim 1.5$ . For  $|y| < 1.5$  pion production greatly dominates proton production and the bias is consequently small.<sup>9</sup>

## II. LOCAL COMPENSATION OF CHARGE AND ZONE STRUCTURE

Zone graphs for typical events at 102 GeV/c and 400 GeV/c are shown in Fig. 1. Each of the events shown contains two end zones and two central zones. The probability for observing an event containing a total of  $N_z$  zones is shown in Fig. 2. The probability distribution at 400 GeV/c is clearly shifted toward higher values of  $N_z$ . In Table I we list the mean  $\langle N_z \rangle$  and dispersion  $(\langle N_z^2 - \langle N_z \rangle^2)^{1/2}$  of these distributions; we also provide these quantities calculated using our model (RCM). The data at both energies contain

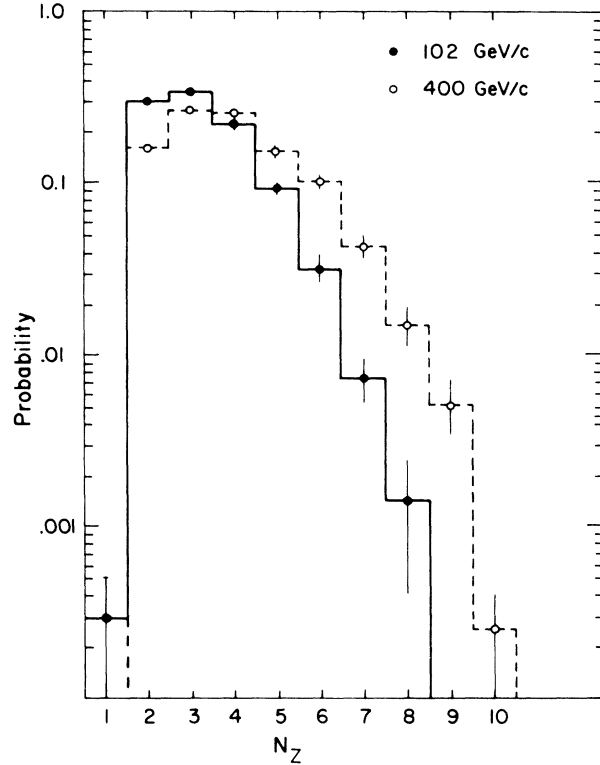


FIG. 2. Probability distributions for the number of zones per event.

more zones per event than is found using the RCM. The data also indicate a faster growth of the mean number of zones with increasing incident momentum than is provided by the RCM; the ratio of the mean number of zones for the two energies  $\langle N_z \rangle_{400} / \langle N_z \rangle_{102}$  is  $1.24 \pm 0.01$  in the data and 1.15 in the model. This rate of growth of  $\langle N_z \rangle$  is somewhat smaller than the increase observed in the mean charged-particle multiplicity ( $\langle n_c \rangle = 6.32 \pm 0.08$  and  $8.96 \pm 0.10$  at 102 and 400 GeV/c, respectively<sup>10</sup>). Dividing the mean charged-particle multiplicity, increased by two units of charge (corresponding to the beam and target "compensating" charges), by  $\langle N_z \rangle$ , one obtains the mean

TABLE I. Zone structure parameters.

All zones	102 GeV/c		400 GeV/c	
	Data	RCM	Data	RCM
$\langle N_z \rangle$	$3.23 \pm 0.02$	2.96	$4.00 \pm 0.03$	3.40
$(\langle N_z^2 - \langle N_z \rangle^2)^{1/2}$	$1.13 \pm 0.01$	1.06	$1.51 \pm 0.01$	1.39
$\langle n_z \rangle$	$2.55 \pm 0.02$	2.81	$2.75 \pm 0.03$	3.24
$\langle \lambda_z \rangle$	$0.97 \pm 0.01$	1.15	$1.00 \pm 0.01$	1.29

number of charges per zone  $\langle n_z \rangle = (\langle n_c \rangle + 2) / \langle N_z \rangle$ ; this quantity increases with  $s$ , indicating that the average internal structure of zones changes somewhat between our two energies. It should be noted, however, that the increase in  $\langle n_z \rangle$  is smaller than expected on the basis of the RCM (see Table I).

The probability distribution of zone lengths,  $\lambda_z$ , is displayed in Fig. 3; corresponding values of the mean  $\langle \lambda_z \rangle$  and dispersion  $(\langle \lambda_z^2 \rangle - \langle \lambda_z \rangle^2)^{1/2}$  are given in Tables I and II. As was the case for  $\langle n_z \rangle$ , the mean rapidity length of zones  $\langle \lambda_z \rangle$  also rises with increasing  $s$  at a rate far smaller than predicted by the RCM (see Table I.) Thus both  $\langle n_z \rangle$  and  $\langle \lambda_z \rangle$  show trends in the direction required by local compensation of charge. The data in Fig. 3 have been separated into end zones and central zones. The difference between the length distribution for these two types of zones can presumably be attributed in large part to the inclusion of the beam and target rapidities in the definition of  $Z(y)$  given in Eq. (1). It is somewhat surprising, however, that the average number of charges  $\langle n_z \rangle$  for end zones does not differ substantially from the result for central zones. This near equality suggests a similar production mechanism for the two types of zones.

Examining separately the behavior of central zones, we find there is essentially no energy dependence observed for the average central zone length  $\langle \lambda_z \rangle$ . The increase in  $\langle \lambda_z \rangle$  from 102 to 400 GeV/c is only  $(1 \pm 1)\%$ , while a growth of 7% is predicted by the RCM. Thus it would appear to be justified to take  $\langle \lambda_z \rangle \approx 0.75$  as the rapidity length over which charge is compensated in the central region. Although this value of  $\langle \lambda_z \rangle$  is remarkably stable, notice that  $\langle n_z \rangle$  for central zones still increases by  $(10 \pm 2)\%$ . Thus the full set of asymptotic conditions required by LCC are not yet accurately satisfied at Fermilab energies.

For completeness, we display in Table III the semi-inclusive zone parameters at 102 and 400 GeV/c. It is clear that the stability observed for inclusive central values of  $\langle \lambda_z \rangle$  is not maintained in the semi-inclusive channels.

Using the generalized charge transfer  $Z(y)$  let us now define a zone correlation function,<sup>5</sup>

$$D(y_1, y_2) = \langle Z(y_1)Z(y_2) \rangle - \langle Z(y_1) \rangle \langle Z(y_2) \rangle, \quad (2)$$

which,<sup>11</sup> when evaluated for  $pp$  collisions at  $y_1 = y_2 = 0$ , yields the variance of the charge transfer across  $y = 0$ :

$$\begin{aligned} D(0, 0) &= \langle Z(0)Z(0) \rangle - \langle Z(0) \rangle \langle Z(0) \rangle \\ &= \langle u^2 \rangle - \langle u \rangle^2 = \langle u'^2 \rangle. \end{aligned} \quad (3)$$

For  $\Delta y = |y_1 - y_2| = 0$  but  $y = y_1 = y_2 \neq 0$ ,  $D(y_1, y_2)$  measures fluctuations in the charge transferred

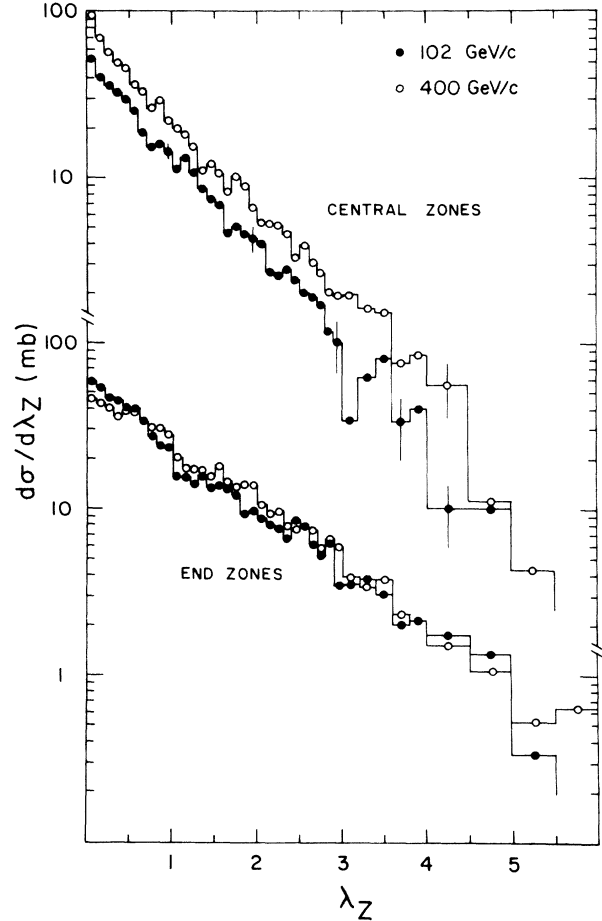


FIG. 3. Distributions in zone lengths.

across  $y$ ; for intermediate values of  $\Delta y$ , e.g.,  $\Delta y \approx \langle \lambda_z \rangle$ ,  $D(y_1, y_2)$  reflects primarily the internal structure of individual zones; and for large  $\Delta y$ , i.e.,  $\Delta y \gg \langle \lambda_z \rangle$ ,  $D(y_1, y_2)$  may be thought of as a gauge of long-range correlations between pairs of zones. Thus, for  $\Delta y = 0$  and for intermediate  $\Delta y$ , the information carried by  $D(y_1, y_2)$  overlaps to a degree

TABLE II. Zone structure for central and end zones.

	102 GeV/c		400 GeV/c	
	Data	RCM	Data	RCM
End zones				
$\langle n_z \rangle$	$2.62 \pm 0.02$	2.94	$2.71 \pm 0.03$	3.43
$\langle \lambda_z \rangle$	$1.10 \pm 0.02$	1.38	$1.24 \pm 0.02$	1.73
Central zones				
$\langle n_z \rangle$	$2.51 \pm 0.02$	2.57	$2.77 \pm 0.03$	2.93
$\langle \lambda_z \rangle$	$0.75 \pm 0.01$	0.78	$0.76 \pm 0.01$	0.84
$(\langle \lambda_z^2 \rangle - \langle \lambda_z \rangle^2)^{1/2}$	$0.73 \pm 0.01$	0.78	$0.80 \pm 0.01$	0.91

TABLE III. Semi-inclusive zone structure parameters.

$n_c$	All zones		Central zones		End zones	
	$\langle n_z \rangle$	$\langle \lambda_z \rangle$	$\langle n_z \rangle$	$\langle \lambda_z \rangle$	$\langle n_z \rangle$	$\langle \lambda_z \rangle$
102 GeV/c						
2	2.00 ± 0.01	0.85 ± 0.04			2.00 ± 0.01	0.85 ± 0.04
4	2.24 ± 0.02	1.01 ± 0.03	2.00 ± 0.01	0.98 ± 0.04	2.32 ± 0.02	1.03 ± 0.03
6	2.45 ± 0.03	1.02 ± 0.02	2.28 ± 0.03	0.91 ± 0.03	2.55 ± 0.03	1.09 ± 0.03
8	2.72 ± 0.03	1.00 ± 0.02	2.52 ± 0.03	0.73 ± 0.02	2.90 ± 0.05	1.23 ± 0.03
10	2.84 ± 0.05	0.88 ± 0.03	2.72 ± 0.08	0.62 ± 0.03	2.97 ± 0.09	1.17 ± 0.04
12	3.25 ± 0.12	0.95 ± 0.06	2.78 ± 0.12	0.54 ± 0.05	3.79 ± 0.20	1.41 ± 0.07
≥14	3.25 ± 0.15	0.78 ± 0.05	3.18 ± 0.20	0.46 ± 0.07	3.49 ± 0.30	1.27 ± 0.08
400 GeV/c						
2	2.00 ± 0.01	0.78 ± 0.07			2.00 ± 0.01	0.78 ± 0.07
4	2.17 ± 0.02	1.03 ± 0.04	2.00 ± 0.01	1.07 ± 0.05	2.24 ± 0.02	1.01 ± 0.04
6	2.35 ± 0.02	1.13 ± 0.03	2.21 ± 0.03	1.01 ± 0.04	2.44 ± 0.03	1.22 ± 0.04
8	2.59 ± 0.03	1.14 ± 0.03	2.46 ± 0.03	0.91 ± 0.03	2.72 ± 0.05	1.34 ± 0.04
10	2.70 ± 0.05	0.98 ± 0.03	2.59 ± 0.05	0.74 ± 0.03	2.85 ± 0.08	1.27 ± 0.05
12	2.92 ± 0.06	0.97 ± 0.03	2.88 ± 0.08	0.74 ± 0.03	2.98 ± 0.10	1.29 ± 0.05
14	3.14 ± 0.09	0.96 ± 0.04	2.99 ± 0.09	0.63 ± 0.03	3.37 ± 0.20	1.46 ± 0.07
16	3.17 ± 0.10	0.88 ± 0.05	3.17 ± 0.15	0.60 ± 0.04	3.17 ± 0.20	1.40 ± 0.09
18	3.33 ± 0.16	0.85 ± 0.07	3.31 ± 0.20	0.53 ± 0.05	3.39 ± 0.30	1.49 ± 0.10
≥20	3.83 ± 0.30	0.83 ± 0.08	3.93 ± 0.30	0.53 ± 0.06	3.14 ± 0.40	1.47 ± 0.10

with the results gotten by examining zone lengths  $\lambda_z$  and multiplicities  $n_z$ , but for large  $\Delta y$ ,  $D(y_1, y_2)$  provides completely new information.

In Fig. 4 we plot  $D(y_1, y_2)$ , evaluated at  $y_1 = 0$ , and  $-1.2$  as functions of  $\Delta y$ ; curves representing the results of the RCM are given for the same  $y$  values. The data have smaller values of  $D(y_1, y_2)$  than provided by the RCM curves; the discrepancy is more pronounced at higher energy. (This implies that the high-multiplicity events do not exhibit the large fluctuations in charge transfer generated by the RCM.) The values of  $D(0, 0)$  are  $0.90 \pm 0.04$  and  $1.12 \pm 0.05$  at 102 and 400 GeV/c, respectively. The small magnitude and the energy dependence of  $D(0, 0)$ , which will be discussed later in terms of a cluster model, are cited here as further evidence for the presence of an LCC mechanism. We also note the rapid, nearly exponential fall of  $D(y_1, y_2)$  as a function of  $\Delta y$ . This exponential behavior again indicates a strong tendency for charge transfer to occur only over small distances in rapidity space. In addition, it implies the absence of significant long-range correlations between separated pairs of zones. The rate at which  $D(y_1, y_2)$  falls with increasing rapidity separation can be characterized by a correlation length  $L$ , where  $D(\Delta y) \approx \exp(-\Delta y/L)$ . We obtain  $L \approx 1.1 - 1.2$ , somewhat larger than the value of the average zone length  $\langle \lambda_z \rangle \approx 0.75$ .

It is probably useful to point out that the well-

known "leading particle effect," which in LCC language is compensation of the charge of incident particles near the edges of rapidity space, cannot explain the main features of the discrepancy between the data and the RCM. For example, fixing the rapidities of the extreme positive particles and randomizing the charges only of the remaining particles reduces the RCM values of  $D(0, 0)$  by  $\approx 0.5$ .<sup>12</sup> The new values, 1.08 and 1.74 at 102 and 400 GeV/c respectively, are still significantly above the data and rise with energy more rapidly.

In the above analysis we have found that parameters describing the statistical properties of zone graphs exhibit regularities which tend to support the LCC hypothesis. When compared to the RCM predictions, the very weak energy dependence of the mean zone length  $\langle \lambda_z \rangle$  and the rapid decrease of the zone correlation function  $D(y_1, y_2)$  with increasing rapidity difference  $\Delta y$  are trends in the direction required by LCC. However, we also find that the mean number of charges per zone  $\langle n_z \rangle$  and the magnitude of the zone correlation function  $D(0, 0) \equiv \langle u^2 \rangle$  rise with increasing  $s$ . These energy variations can be attributed, at least in part, to the growth of the single-particle densities in the Fermilab energy range. Because the latter feature of the data is ignored in the asymptotic forms of simple multiperipheral cluster models as well as the LCC hypothesis, we anticipate that simple cluster

models will also fail to provide a complete account of the observed energy variations of charge distributions.

### III. CHARGE TRANSFERS ACROSS $y = 0$

The independent neutral-cluster emission model is one of a large class of models which satisfy the LCC hypothesis. In this section we compare the data for charge transfer across  $y = 0$  with a cluster model of this sort investigated by Quigg and Thomas.<sup>2</sup> The model assumes multiperipheral production of neutral clusters which subsequently decay into a fixed number of pions; the decay pions are dispersed over a finite region of rapidity space. Quigg and Thomas prove the following results for the functional dependences of charge-transfer parameters in their model:

$$\langle u^2 \rangle = \frac{K}{Y} \langle N \rangle, \quad (4a)$$

$$\langle u_{l^-, r^-} \rangle = \frac{K}{Y} (l^- - r^-), \quad (4b)$$

$$\langle u_{l^-, r^-}^2 \rangle - \langle u_{l^-, r^-} \rangle^2 = \frac{K}{Y} \left(1 - \frac{K}{Y}\right) (l^- + r^-). \quad (4c)$$

The notation is as follows:  $Y$  is the total range of rapidities;  $\langle N \rangle$  is the mean number of clusters;  $l^-$  and  $r^-$  are respectively the number of negative particles emitted into the left and right (backward and forward) center-of-mass hemispheres;  $K$  is a constant which depends only on the nature of the cluster decay. The value of  $\langle N \rangle$  is assumed to grow logarithmically with  $s$  (i.e., a constant cluster density,  $\langle N \rangle / Y$ , is assumed); consequently the value of  $\langle u^2 \rangle$  is expected to approach a constant at high energies. (Note that  $\langle u^2 \rangle$  contains an averaging over all events, while the subscripted  $u$  variables are averages over fixed multiplicity.) The magnitude of  $\langle u^2 \rangle$  has already been shown to differ significantly from that expected for a random charge distribution; here we note that the energy dependence of  $\langle u^2 \rangle$ , given in Fig. 5, does not yet suggest an approach to a constant value.<sup>13</sup> Since, as we have already mentioned, there is no evidence at the energies we are considering for an  $s$ -independent rapidity plateau, which is assumed in the model of Quigg and Thomas, a slow increase in  $\langle u^2 \rangle$  is not surprising. (The single-particle invariant cross sections at  $y = 0$ , integrated over transverse momenta, are  $48.3 \pm 2.5$  and  $64.6 \pm 3.2$  mb at 102 and 400 GeV/c, respectively.)

Charge-transfer properties as a function of charged-prong multiplicity are given in Table IV and in Figs. 6 and 7. In obtaining these data we have made use of the symmetry about  $y = 0$  expected

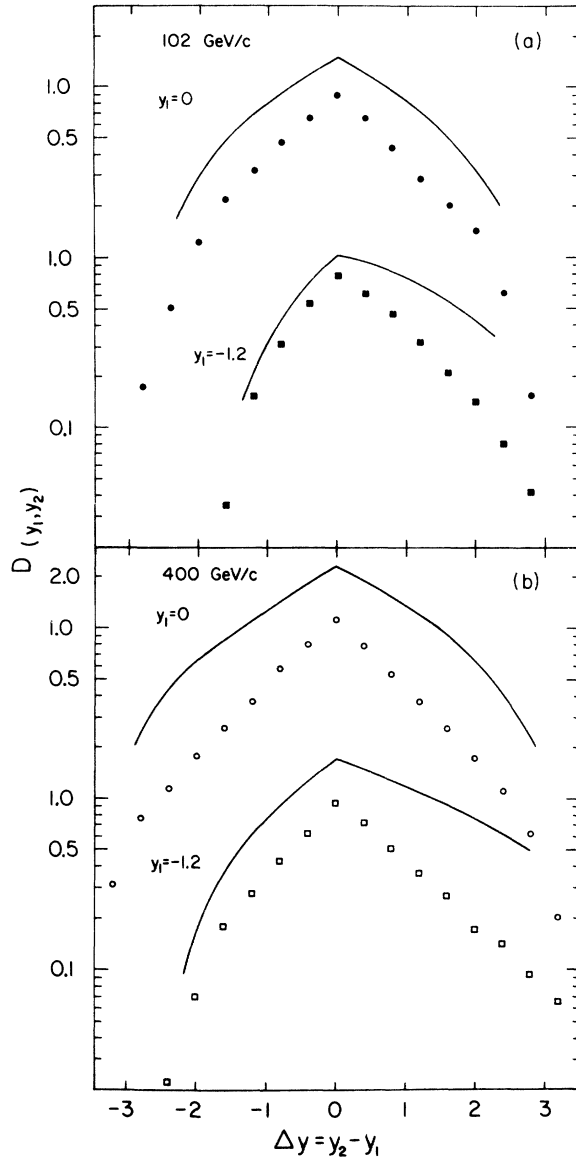


FIG. 4. The correlation function  $D(y_1, y_2)$  evaluated at  $y_1 = 0$  and  $y_1 = -1.2$  as a function of  $\Delta y$ . The curves are the results of randomizing the charge distributions in each event (RCM described in the text).

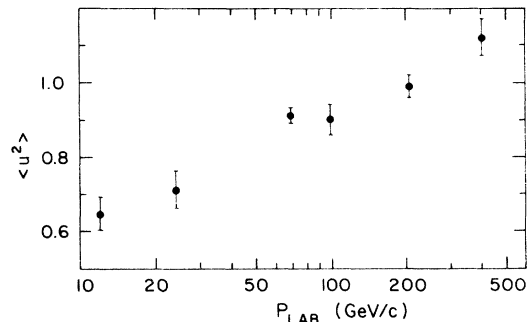


FIG. 5. Energy dependence of  $\langle u^2 \rangle$ .

TABLE IV. Charge-transfer averages.

$n_c$	$l^-$	$r^-$	102 GeV/c		400 GeV/c	
			$\langle u_{l^-,r^-} \rangle$	$\langle u_{l^-,r^-}^2 \rangle - \langle u_{l^-,r^-} \rangle^2$	$\langle u_{l^-,r^-} \rangle$	$\langle u_{l^-,r^-}^2 \rangle - \langle u_{l^-,r^-} \rangle^2$
2	0	0	$-0.02 \pm 0.02$	$0.17 \pm 0.02$	$-0.01 \pm 0.03$	$0.09 \pm 0.02$
4	1	0	$0.24 \pm 0.02$	$0.41 \pm 0.02$	$0.26 \pm 0.03$	$0.31 \pm 0.03$
6	2	0	$0.62 \pm 0.04$	$0.62 \pm 0.04$	$0.49 \pm 0.05$	$0.53 \pm 0.05$
	1	1	$0.09 \pm 0.04$	$0.62 \pm 0.04$	$0.07 \pm 0.05$	$0.52 \pm 0.05$
8	3	0	$1.15 \pm 0.08$	$0.89 \pm 0.10$	$0.92 \pm 0.08$	$0.91 \pm 0.09$
	2	1	$0.36 \pm 0.05$	$0.86 \pm 0.06$	$0.23 \pm 0.05$	$0.82 \pm 0.06$
10	4	0	$1.3 \pm 0.2$	$1.6 \pm 0.6$	$1.0 \pm 0.2$	$1.1 \pm 0.2$
	3	1	$0.87 \pm 0.11$	$1.1 \pm 0.2$	$0.44 \pm 0.09$	$0.90 \pm 0.10$
	2	2	$0.18 \pm 0.09$	$0.79 \pm 0.10$	$0.03 \pm 0.11$	$1.10 \pm 0.16$
12	5	0	$2.3 \pm 0.3$	$0.90 \pm 0.35$	$1.2 \pm 0.3$	$1.3 \pm 0.5$
	4	1	$1.0 \pm 0.3$	$1.2 \pm 0.3$	$1.05 \pm 0.14$	$1.14 \pm 0.22$
	3	2	$0.39 \pm 0.14$	$1.2 \pm 0.2$	$0.12 \pm 0.10$	$1.04 \pm 0.14$
14	6	0			$1.6 \pm 0.4$	$1.3 \pm 0.4$
	5	1	$1.5 \pm 0.4$	$1.1 \pm 0.4$	$1.1 \pm 0.2$	$0.75 \pm 0.20$
	4	2	$0.8 \pm 0.4$	$1.7 \pm 0.9$	$0.65 \pm 0.15$	$1.3 \pm 0.2$
	3	3	$0.3 \pm 0.4$	$0.9 \pm 0.6$	$-0.14 \pm 0.20$	$1.4 \pm 0.3$
16	7	0				
	6	1				
	5	2			$0.74 \pm 0.23$	$0.98 \pm 0.32$
	4	3	$0.1 \pm 0.5$	$2.1 \pm 0.8$	$-0.12 \pm 0.20$	$1.7 \pm 0.4$
18	8	0				
	7	1				
	6	2			$2.1 \pm 0.3$	$1.0 \pm 0.4$
	5	3			$0.23 \pm 0.36$	$1.6 \pm 0.9$
	4	4			$0.00 \pm 0.4$	$2.4 \pm 0.9$

for  $pp$  collisions. For example, in the eight-pronged topology the value of  $\langle u_{2,1} \rangle$  has been averaged with  $-\langle u_{1,2} \rangle$ . This folding procedure tends to reduce the systematic biases in the data due to proton/pion misidentification near  $y=0$ . We have not corrected the symmetric entries in Table IV (e.g.,  $\langle u_{1,1} \rangle$ ) for this known bias, and consequently the deviations from  $\langle u_{m,m} \rangle = 0$  provide a measure of the systematic uncertainties in our measurements. (The errors given in Table IV are statistical.)

In Figs. 6(a) and 6(b) we present the dependence of  $\langle u_{l^-,r^-} \rangle$  on  $(l^- - r^-)$  and the dependence of  $\langle u_{l^-,r^-}^2 \rangle - \langle u_{l^-,r^-} \rangle^2$  on  $(l^- + r^-)$ . The straight lines given in Fig. 6 are expectations based on the independent-emission model (IEM)—i.e., the independent emission of single pions rather than pion clusters.<sup>1,2</sup> The  $s$ -independent rather than pion clusters.<sup>1,2</sup> The  $s$ -independent expressions in the IEM are  $\langle u_{l^-,r^-} \rangle = \frac{1}{2}(l^- - r^-)$ , and  $\langle u_{l^-,r^-}^2 \rangle - \langle u_{l^-,r^-} \rangle^2 = \frac{1}{4}(l^- + r^-)$ ; these simple forms are very close to the RCM values with the “leading particle effect” removed.

The data in Fig. 6(a) lie below the IEM prediction, indicating the presence of substantial clustering.

The linear dependence predicted by the cluster model [ Eq. 4 (b) ] is consistent with the data; however, the significant scatter in  $\langle u_{l^-,r^-} \rangle$  at fixed  $(l^- - r^-)$  and fixed  $s$  cannot be understood on the basis of the simple model of Ref. 2.

In Fig. 6(b) we again note discrepancies between predictions of the IEM and the data. In particular, for  $n_- = l^- + r^- < 3$  the data are above the curve, indicating the presence of diffractive “spillover” contributions near  $y=0$ .<sup>1</sup> For  $n_- > 3$  the data are statistically poor; nevertheless they clearly lie below the IEM line, suggesting the presence of clustering effects [ Eq. 4(c) ].

We investigate the energy dependence of  $\langle u_{l^-,r^-} \rangle$  in Fig. 7, where the data from this and other experiments<sup>14, 15</sup> for  $r^- = 0$  are plotted. The  $s$  dependence is consistent with a  $1/\ln s$  form [ Eq. 4(b) ] and extrapolates reasonably to  $\langle u_{l^-,r^-} \rangle = 0$  for all available data.

Although parameters relating to cluster properties can be extracted from the data presented in this paper (e.g., an average of 2–2.5 charged particles per cluster), the precise values obtained

for these parameters are sensitive to model-dependent corrections resulting from the nonasymptotic energies of Fermilab.

IV. SUMMARY

We have presented new results on the charge structure of final states observed in  $pp$  collisions at 102 and 400 GeV/c. We find significant deviations from the assumption of random charge distribution. These deviations are in the direction required by the hypothesis that local compensation of charge is fulfilled asymptotically at high energies. The neutral-cluster model which we examined is able to account for the general features of our data for the charge transfer  $u$ . However, neither the predictions of LCC for the full charge structure of events nor the predictions of the neutral-cluster model for the charge transfer  $u$  are in complete agreement with the data. We attribute this lack of detailed agreement, at least in part, to the nonasymptotic nature of Fermilab energies.

ACKNOWLEDGMENTS

We thank A. Krzywicki for helpful correspondence, and C. Quigg for comments on this work.

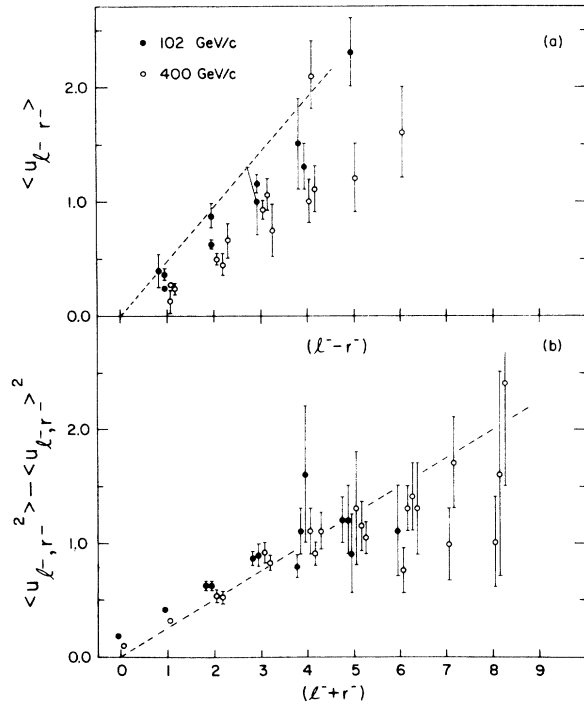


FIG. 6. (a) The mean of the charge transfer for fixed  $l^-$  and  $r^-$  as a function of the difference  $l^- - r^-$ . (b) The variance of the charge transfer for fixed  $l^-$  and  $r^-$  as a function of the sum  $l^- + r^-$ . Expectations for models with independent emission of single pions (Ref. 1,2) are given by dashed lines.

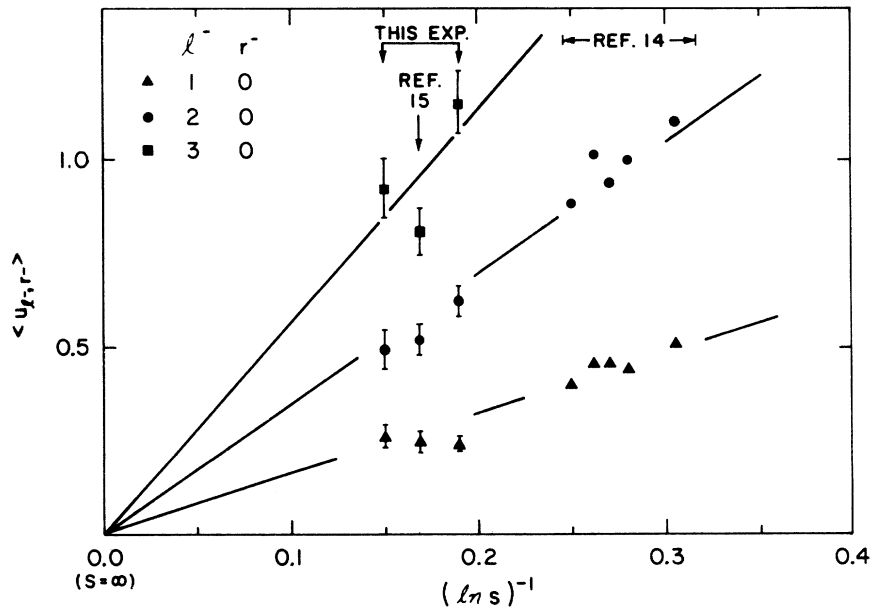


FIG. 7. Energy dependence of the mean charge transfer for fixed  $l^-$  where  $r^- = 0$ . The  $(\ln s)^{-1}$  dependence expected in the cluster model is shown by straight lines passing through the origin.

\*Work supported in part by the U. S. Energy Research and Development Administration.

†Present address: Stanford University, Stanford, Calif. 94305.

<sup>1</sup>T. T. Chou and C. N. Yang, Phys. Rev. D 7, 1425 (1973).

<sup>2</sup>C. Quigg and G. H. Thomas, Phys. Rev. D 7, 2752 (1973).

<sup>3</sup>D. Sivers and G. H. Thomas, Phys. Rev. D 9, 208 (1974).

<sup>4</sup>A. Krzywicki and D. Weingarten, Phys. Lett. 50B, 265 (1974).

<sup>5</sup>D. Weingarten, Phys. Rev. D 11, 1924 (1975).

<sup>6</sup>A. Krzywicki, Nucl. Phys. B86, 296 (1975).

<sup>7</sup>For an examination of  $pp$  data at 69 GeV/c in terms of the LCC hypothesis, see J. Derré *et al.*, French-Soviet Collaboration Report No. M12, 1974 (unpublished).

<sup>8</sup>C. Bromberg *et al.*, Phys. Rev. D 9, 1864 (1974).

<sup>9</sup>The size of the bias can be gauged by the small positive

values for  $\langle u \rangle$ ,  $0.07 \pm 0.02$  at 102 GeV/c and  $0.03 \pm 0.03$  at 400 GeV/c; both numbers are consistent with estimates for the effects of proton contamination near  $y=0$ . See also Ref. 8.

<sup>10</sup>C. Bromberg *et al.*, Phys. Rev. Lett. 31, 1563 (1973); 32, 83 (1974).

<sup>11</sup>The diagonal part of  $D(y_1, y_2)$  is identical to a function defined by R. Baier and F. W. Bopp in a discussion of a neutral-cluster model [University of Bielefeld Report No. BI 74/06, 1974 (unpublished)].

<sup>12</sup>For completely uncorrelated charged-particle production,  $D(0,0)$  is given by  $n_c/4$ , consistent with the results of our RCM simulation.

<sup>13</sup>References for the data in Fig. 5 are U. Idschok *et al.*, Nucl. Phys. B67, 93 (1973); J. Derré *et al.*, Ref. 7 (69 GeV/c); M. Pratap, private communication (205 GeV/c).

<sup>14</sup>The MSU data are from Ref. 1 and from a private communication of B. Y. Oh.

<sup>15</sup>T. Kafka *et al.*, Phys. Rev. Lett. 34, 687 (1975).